JOURNAL OF GUIDANCE, CONTROL, AND DYNAMICS
Vol. 24, No. 2, March–April 2001

Two-Timescale Inverse Simulation of a Helicopter Model

Giulio Avanzini*
Polytechnic of Turin, 10129 Turin, Italy
and
Guido de Matteis†
University of Rome "La Sapienza," 00184 Rome, Italy

The objective is the development and evaluation of a fast and reliable, multiple-timescale algorithm for the inverse simulation of rotorcraft maneuvering tasks. A recent, two-timescale approach to the solution of inverse problems of aircraft motion represents the background for devising a technique that accounts for specific issues of rotorcraft dynamics such as the large effects of the fast, primary moment generating controls on the slow dynamics associated to the vehicle trajectory and the system being frequently nonminimum phase. Accurate solutions are obtained for the inverse simulations of the fast and slow reduced-order systems because the quasi-steady-state values of the fast controls are considered in the slow timescale. High-amplitude oscillations in the control inputs, revealed in previous applications of helicopter inverse simulation, are interpreted as due to the presence of nonobservable motions and are ruled out by the multiple timescale approach. The results show that the expected computer time reduction is realized, that the well-known difficulties of inverse methods for finding feasible solutions at convergence are practically eliminated, and, finally, that steady-state flight conditions are accurately recovered at the end of the prescribed maneuvers.

Nomenclature

g	=	gravity acceleration
I_x, I_y, I_z	=	moments of inertia
I_{xz}	=	product of inertia
k_1, k_2	=	curvature and torsion
L, M, N	=	moment components in body axes
$\mathcal{L}_i, \mathcal{M}_i, \mathcal{N}_i$	=	dimensional derivatives due to state or input i
$\boldsymbol{L}_{IF}, \boldsymbol{L}_{IB}$	=	transformation matrices
m	=	helicopter mass
N	=	number of fast timescale intervals inside Δt
$\boldsymbol{n}$	=	normal unit vector
$\boldsymbol{R}$	=	inertial coordinate vector (north, east and down), $(R_N, R_E, R_D)^T$
s	=	curvilinear abscissa
t	=	time
u, v, w	=	velocity components in body axes
$\boldsymbol{u}$	=	control vector
V	=	velocity modulus
$\boldsymbol{V}$	=	inertial velocity vector, $(V_N, V_E, V_D)^T$
X, Y, Z	=	force components in body axes
$\boldsymbol{x}$	=	state vector
$\boldsymbol{y}$	=	output vector
α	=	angle of attack, $\tan^{-1}(w/u)$
β	=	sideslip angle, $\sin^{-1}(v/V)$
Δt	=	time interval of the slow dynamics
δ_A	=	lateral cyclic stick movement, positive right
δ_B	=	longitudinal cyclic movement, positive after or nose-up
δ_C	=	collective control input, positive up
δ_P	=	pedal movement, positive left or nose-left
δt	=	time interval of the fast dynamics
$\delta\eta$	=	time step for the numerical integration
$\delta\tau$	=	time delay
ϵ	=	perturbation parameter
$\boldsymbol{\xi}$	=	c.g. position in the Frenet triedron
ρ	=	air density
ϕ, θ, ψ	=	Euler's angles
$\boldsymbol{\omega}$	=	angular velocity vector, $(p, q, r)^T$

Subscripts

des	=	desired
e	=	steady state
F	=	fast timescale
S	=	slow timescale

Superscript

$'$	=	displacement from trim value

Presented as Paper 99-4112 at the AIAA Atmospheric Flight Mechanics Conference, Portland, OR, 9–11 August 1999; received 17 September 1999; revision received 11 May 2000; accepted for publication 13 May 2000.

*Research Scientist, Department of Aerospace Engineering, corso Duca degli Abruzzi 24. Member AIAA.

†Professor, Department of Mechanics and Aeronautics, via Eudossiana 18. Member AIAA.

I. Introduction

A TWO-TIMESCALE integration technique is proposed for the inverse simulation of a helicopter model in maneuvering flight. Inverse simulation is a means for generating forward control inputs such that the model would perfectly track the assigned flight path, if feasible, in the absence of modeling errors and disturbances. Among the large number of applications of the method in flight mechanics and with reference to rotorcraft models are the evaluation of agility,[1] the validation of theoretical models,[2] the analysis of maximum maneuvering performances,[3] the formulation of task driven bandwidth requirements for the design of stability augmentation systems,[4] the investigation of the effect of engine failures during takeoff from offshore platforms,[5] and the assessment of handling qualities.[6] In Ref. 7, where a maneuver autopilot of an autonomous vehicle is dealt with, an inverse problem is solved to determine the feedforward control variables for optimal tracking of a commanded acceleration. The algorithm for the inverse simulation is coupled with a robust tracking controller to account for parameter uncertainties and atmospheric turbulence. The technique in Ref. 7 appears as a computationally efficient and relatively simple approach to the design of trajectory tracking controllers for low-cost remotely piloted vehicles suitable for aeronautical research activities.

Solving the equations of motion of the vehicle in an inverse manner is not a trivial task, and many problems are frequently encountered. Issues such as numerical stability and accuracy, computational time, and reliability of the algorithm are taken into consideration. The studies in Refs. 8–12 provide an extensive discussion concerning several numerical aspects to be addressed for a successful implementation of the main techniques used in inverse simulation.

Inverse simulation of helicopter motion presents some distinctive issues related to the rather complex model of the vehicle, where either tip-path plane or multiblade descriptions of quasi-steady main rotor flapping, quasi-steady inflow dynamics,[4,6] and in more sophisticated applications[13] a dynamic model of the individual rotor blades are featured, depending on the required maneuvering tasks. In this context, the so-called integration technique deserves interest mainly because it is capable of accommodating different mathematical models without restructuring the algorithm. In the integration method, the control variables are modified in an iterative fashion until the output variables, computed by numerical integration of the equations of motion over the discretization interval δt, are brought to the desired values.

In this study, the inverse simulation of the four-dimensional (a three-dimensional trajectory assigned as a function of time) tracking of a helicopter model is carried out in the framework of a recent method[11] based on the integration approach and the timescale separation (TSS) concept.[14] The principal advantages of the technique, as compared with the original integration algorithm,[4] are a significant reduction of the computational time and the elimination of numerical stability problems, that is, high-amplitude, high-frequency oscillations and an inherent difficulty to find converged solutions, which can be very restrictive, particularly when multiple timescales are present in the vehicle dynamics,[9] as well as in nonminimum-phase systems.[10,11]

As relevant features, in the context of feedforward maneuver control, the method utilizes a three-dimensional trajectory specified in the inertial reference frame as input, accounts for model nonlinearities, and can handle performance and actuator limitations. On the other hand, the present approach is not suitable for those applications, that is, highly aggressive maneuvers or simulations at the extremes of the flight envelope,[13] where additional timescales such as the high bandwidth dynamics of individual blades and actuators are excited.

The adoption of the TSS technique[11] for the inverse simulation of helicopter maneuvers is far from straightforward. We retain the basic assumption of the TSS approach that the collective is a force control associated to the slow timescale, whereas the cyclic and the directional are attitude controls related to the fast dynamics. The next step in most of the reported applications of TSS[15,16] is to assume that the fast timescale controls produce negligible body forces. It has been demonstrated in Ref. 15 that the effects of the fast inputs on the slow dynamics can be neglected where fixed wing aircraft models are dealt with. However, the rationale for this simplification is to be carefully substantiated when helicopter models are considered because significant body forces are generated by cyclic stick (δ_A and δ_B) and pedals (δ_P) due to main rotor disk tilting and tail rotor collective pitch variation, respectively. In this respect, the synthesis of a trajectory controller in Ref. 16, where the singular perturbation theory[14] (SPT) is used for separating the helicopter dynamics into slow and fast models, is conducted using a very simple model of the vehicle, and the effects on the slow dynamics caused by the aforementioned approximation are not investigated. We show that the full model of the helicopter can be decoupled into two lower-order models provided that the force terms due to the inputs δ_A, δ_B, and δ_P are incorporated in the governing equations of the slow timescale. Note that, when severe maneuvers are performed, some coupling between the slow and fast dynamics results from the effects of the helicopter rotational velocity on the rotor and body forces.

Further concerns are related to the behavior of internal states when the elements of the observation vector, that is, the vector of desired outputs, are trajectory variables, that is, the c.g. inertial coordinates. In this circumstance, even though the assigned outputs are accurately achieved, the helicopter model may exhibit undamped oscillations when the computed control law is used as an input for the forward simulation of the assigned maneuver. As a consequence, steady-state conditions cannot be recovered for the full state at the end of the prescribed maneuver. This is not a negligible issue when, for instance, feedforward commands are to be generated for a trajectory controller. This kind of behavior, clearly visible in the inverse simulation results of Ref. 4, is explained here as caused by the presence of conjugate transmission zeros close to the imaginary axis, so that there exist not observable oscillatory motions.

In the proposed method, we consider the two timescales of the TSS approach as discussed, among many others, in Refs. 14–16. Accordingly, the principal results of the SPT are recalled to formulate two subproblems for the slow and fast timescales of the helicopter dynamics. Then, the c.g. location along the trajectory is expressed, in the Frenet triad, as a power series expansion[17] in term of the curvilinear abscissa s and, as a result, the slow control inputs are determined by solving an algebraic problem. Finally, the fast timescale control variables are calculated by a local optimization technique[18] that relies on the integration method. In our application, we use a model of the Bell AH-1G single rotor helicopter and determine the control inputs for completing hurdle-hop, slalom, side-step, and accelerating turn maneuvers. The results are discussed in terms of numerical accuracy and computational time.

II. Analysis

In this section the governing equations of the helicopter motion are presented. Then, the singular perturbation approach is used to decompose the full model dynamics. Finally, we add some details on the TSS process by demonstrating that the forces generated by the fast controls cannot be neglected when a rotorcraft model is dealt with.

The desired outputs for the inverse simulation are the inertial coordinates of the vehicle c.g., namely, $[R_N(t),\ R_E(t),\ R_D(t)]_{\text{des}}$. The six-degree-of-freedom equations of motion of the helicopter model, for flat Earth and zero ambient wind, are as follows:

$$\begin{bmatrix} \dot{V}_N \\ \dot{V}_E \\ \dot{V}_D \end{bmatrix} = \frac{1}{m} \boldsymbol{L}_{IB} \begin{bmatrix} X \\ Y \\ Z \end{bmatrix} + \begin{bmatrix} 0 \\ 0 \\ g \end{bmatrix} \tag{1}$$

$$\begin{bmatrix} \dot{R}_N \\ \dot{R}_E \\ \dot{R}_D \end{bmatrix} = \boldsymbol{V} \tag{2}$$

$$\begin{bmatrix} \dot{p} \\ \dot{q} \\ \dot{r} \end{bmatrix} = \begin{bmatrix} \left(A_p J_z + A_r J_{xz}\right) \Big/ \left(J_x J_z - J_{xz}^2\right) \\ \left[J_{xz}(r^2 - p^2) + (J_z - J_x) pr + M\right] \Big/ J_y \\ \left(A_r J_x + A_p J_{xz}\right) \Big/ \left(J_x J_z - J_{xz}^2\right) \end{bmatrix} \tag{3}$$

where

$$A_p = J_{xz} pq + (J_y - J_z) qr + L$$

$$A_r = -J_{xz} qr + (J_x - J_y) pq + N$$

and

$$\begin{bmatrix} \dot{\phi} \\ \dot{\theta} \\ \dot{\psi} \end{bmatrix} = \begin{bmatrix} 1 & \sin\phi \tan\theta & \cos\phi \tan\theta \\ 0 & \cos\phi & -\sin\phi \\ 0 & \sin\phi \sec\theta & \cos\phi \sec\theta \end{bmatrix} \begin{bmatrix} p \\ q \\ r \end{bmatrix} \tag{4}$$

The forces, X, Y, and Z, and moments, L, M, and N, in Eqs. (1) and (3) are in the body-fixed frame and depend on the density $\rho(R_D)$, the linear and angular velocity components, u, v, and w and p, q, and r, respectively, and the control variables δ_A, δ_C, δ_B, and δ_P. In concise state-space form, we write Eqs. (1–4) as

$$\dot{\boldsymbol{x}} = \boldsymbol{f}(\boldsymbol{x}, \boldsymbol{u}) \tag{5}$$

where $\boldsymbol{x} = (V_N, V_E, V_D, p, q, r, \phi, \theta, \psi, R_N, R_E, R_D)^T \in R^{12}$ and $\boldsymbol{u} = (\delta_A, \delta_B, \delta_C, \delta_P)^T \in R^4$. When we consider that the translational dynamics are slow as compared to the attitude dynamics, system (5) can be represented in the well-known singular perturbation form

$$\dot{\boldsymbol{x}}_S = \boldsymbol{h}(\boldsymbol{x}_S, \boldsymbol{x}_F, \boldsymbol{u}_S, \boldsymbol{u}_F; \epsilon) \tag{6}$$

$$\epsilon \dot{\boldsymbol{x}}_F = \boldsymbol{g}(\boldsymbol{x}_S, \boldsymbol{x}_F, \boldsymbol{u}_S, \boldsymbol{u}_F; \epsilon) \tag{7}$$

where $\boldsymbol{x}_S = (V_N, V_E, V_D, R_N, R_E, R_D)^T$ and $\boldsymbol{x}_F = (p, q, r, \phi, \theta, \psi)^T$ are the state vectors of the slow and fast timescale, respectively, and ϵ is a small parameter. In Eqs. (6) and (7), the control vector is partitioned as $\boldsymbol{u} = (\boldsymbol{u}_S, \boldsymbol{u}_F)^T$, where $\boldsymbol{u}_S = [\delta_C]$ and

$\boldsymbol{u}_F = (\delta_A, \delta_B, \delta_P)^T$ because the relevant assumption is made that the collective is a primarily force generating control, whereas the moments are directly controlled by cyclic stick and the pedals.[16] In the slow timescale, we can define the vector of desired outputs as $\boldsymbol{y}_{S_{\text{des}}} = [R_{N_{\text{des}}}(t), R_{E_{\text{des}}}(t), R_{D_{\text{des}}}(t)]^T$.

The slow timescale model is obtained by setting $\epsilon = 0$ in Eqs. (6) and (7). This implies that the fast dynamics are so rapid that the fast states have reached a quasi-steady state in the slow timescale, that is, $\dot{\bar{\boldsymbol{x}}}_F = 0$. Therefore, from Eq. (7) we have

$$\boldsymbol{g}(\bar{\boldsymbol{x}}_S, \bar{\boldsymbol{x}}_F, \bar{\boldsymbol{u}}_S, \bar{\boldsymbol{u}}_F; 0) = 0 \tag{8}$$

where $\bar{\boldsymbol{x}}_F$ and $\bar{\boldsymbol{u}}_F$ represent the slow timescale value of the fast states and controls, respectively. The algebraic Eq. (8), solved in term of the angular velocity, yields from Eqs. (4)

$$\bar{\omega} = 0 \tag{9}$$

whereas, by setting $\dot{\bar{\omega}} = 0$ in Eq. (3), we have

$$\bar{\boldsymbol{u}}_F = \boldsymbol{G}(\bar{\boldsymbol{x}}_F, \bar{\boldsymbol{x}}_S, \bar{\boldsymbol{u}}_S) \tag{10}$$

where $\bar{\boldsymbol{x}}_F(t) = [0, 0, 0, \bar{\phi}(t), \bar{\theta}(t), \bar{\psi}(t)]^T$. Equation (10) allows $\bar{\boldsymbol{u}}_F(t)$ to be expressed as a function of $\bar{\boldsymbol{x}}_F(t)$ and the slow timescale states and controls. By substituting Eq. (10) in Eq. (6), we obtain

$$\dot{\bar{\boldsymbol{x}}}_S = \boldsymbol{h}[\bar{\boldsymbol{x}}_S, \bar{\boldsymbol{x}}_F, \bar{\boldsymbol{u}}_S, \boldsymbol{G}(\bar{\boldsymbol{x}}_F, \bar{\boldsymbol{x}}_S, \bar{\boldsymbol{u}}_S); 0] \tag{11}$$

We consider the augmented slow timescale control vector $\tilde{\boldsymbol{u}}_S(t) = [\bar{\boldsymbol{u}}_S(t), \bar{\phi}(t), \bar{\theta}(t), \bar{\psi}(t)]^T$, where the Euler angles represent pseudo-controls, so that the slow timescale (outer) problem is approximated as follows:

$$\dot{\bar{\boldsymbol{x}}}_S = \boldsymbol{h}(\bar{\boldsymbol{x}}_S, \tilde{\boldsymbol{u}}_S) \tag{12}$$

Turning to the fast timescale (inner) problem, we write from Eq. (7)

$$\dot{\boldsymbol{x}}_F = \boldsymbol{g}(\bar{\boldsymbol{x}}_S, \boldsymbol{x}_F, \bar{\boldsymbol{u}}_S, \boldsymbol{u}_F) \tag{13}$$

where $\bar{\boldsymbol{x}}_S(t)$ and $\bar{\boldsymbol{u}}_S(t)$ are known from the slow timescale. The fast timescale dynamics is required to track the commanded Euler angles as computed in the outer solution, that is, $\boldsymbol{y}_{F_{\text{des}}} = [\bar{\phi}(t), \bar{\theta}(t), \bar{\psi}(t)]^T$.

An important point concerns the influence of the fast states and controls on the slow dynamics. The forces generated by the fast controls are neglected in many reported applications of the SPT in flight dynamics. This rather strong assumption allows for a significant simplification of the outer problem because the solution of Eq. (10), to determine the quasi-steady-state values of the fast controls, is not required. Also, we have that in the TSS approach the forces produced by the angular rate of the vehicle are zero because $\bar{\omega} = 0$ in the slow timescale.

In the sequel, the effects of $\boldsymbol{u}_F$ and $\boldsymbol{\omega}$ as force-generating variables are investigated in the case of a helicopter with articulated rotor. In so doing, and following the approach of Snell et al.,[15] we consider a motion in the vertical plane, where the sideslip angle is zero and the lateral forces and moments are balanced. For a single rotor helicopter there are no purely longitudinal maneuvers, but it appears reasonable in this case to neglect the influence of roll and yaw rates on the longitudinal dynamics. Accordingly, by assuming that the aerodynamic model is affine in the pitch rate q and the input δ_B, the forces X and Z and the moment M are defined by

$$\begin{bmatrix} X \\ Z \\ M \end{bmatrix} = \begin{bmatrix} X_0(u, w, \delta_C) \\ Z_0(u, w, \delta_C) \\ M_0(u, w, \delta_C) \end{bmatrix} + \begin{bmatrix} X_q(u, w) \\ Z_q(u, w) \\ M_q(u, w) \end{bmatrix} q + \begin{bmatrix} X_{\delta_B}(u, w) \\ Z_{\delta_B}(u, w) \\ M_{\delta_B}(u, w) \end{bmatrix} \delta_B \tag{14}$$

where the terms X_0, Z_0, and M_0 depend on slow states and control only. The pitch moment equation can be inverted as follows, to express the longitudinal stick displacement as a function of pitch acceleration and pitch rate:

$$\delta_B = [1/M_{\delta_B}(u, w)][I_y \dot{q} - M_0(u, w, \delta_C) - M_q(u, w) q] \tag{15}$$

On substitution of δ_B in the normal force equation, written for symmetric flight, we have

$$\dot{w} = g \cos\theta + uq + \frac{Z_0(u, w, \delta_C) + Z_q(u, w) q}{m} + \frac{Z_{\delta_B}(u, w)}{m M_{\delta_B}(u, w)} [I_y \dot{q} - M_q(u, w) q - M_0(u, w, \delta_C)] \tag{16}$$

Manipulating Eq. (16) yields

$$\dot{w} = g \cos\theta + (1 + \epsilon_1)[Z_0(u, w, \delta_C)/m] + (1 + \epsilon_2 + \epsilon_3)(q - \epsilon_4 \dot{q}) u \tag{17}$$

where

$$\epsilon_1 = -\frac{Z_{\delta_B}(u, w) M_0(u, w, \delta_C)}{Z_0(u, w, \delta_C) M_{\delta_B}(u, w)}$$

$$\epsilon_2 = -\frac{Z_{\delta_B}(u, w) M_q(u, w)}{mu M_{\delta_B}(u, w)}, \qquad \epsilon_3 = \frac{Z_q(u, w)}{mu}$$

$$\epsilon_4 = \frac{I_y Z_{\delta_B}(u, w)}{Z_{\delta_B}(u, w) M_q(u, w) - M_{\delta_B}(u, w)[mu + Z_q(u, w)]}$$

Provided that $\dot{q}$ and q are specified, the direct effect on the normal acceleration $\dot{w}$ caused by the force generated by the fast control δ_B and state q can be estimated using Eq. (17), where small values of the terms ϵ_1, ϵ_2, ϵ_3, and ϵ_4 indicate that longitudinal cyclic and pitch rate provide a marginal contribution to the slow dynamics. In Fig. 1 the values assumed by ϵ_1, ϵ_2, and ϵ_4 (Fig. 1a) and ϵ_3 (Fig. 1b) are reported as computed for the AH-1G rotorcraft model during a hurdle-hop maneuver, the description of which is given in Sec. IV. It is apparent from Fig. 1a that, at least for the considered maneuver, ϵ_1, ϵ_2, and ϵ_4 are not negligible with respect to unity. As a consequence, the body forces generated by the fast controls should be accounted for in the inverse simulation of rotorcraft motion. On the other hand, Fig. 1b shows that the contribution to the total force of the terms depending on the angular rate is small because the maximum value of ϵ_3 is below 3.3×10^{-3}, and therefore, we can retain $\bar{\omega} = 0$ in

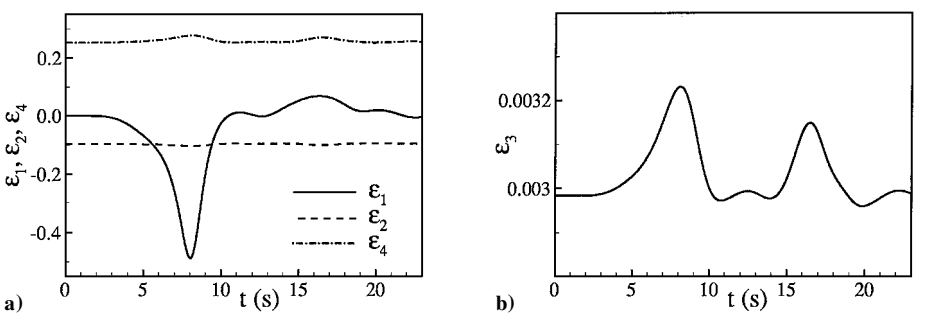

Fig. 1 Variation of ϵ_1, ϵ_2, ϵ_3, and ϵ_4 during a hurdle-hop maneuver.

the outer problem without a significant reduction of accuracy in the trajectory evaluation.

Because the preceding analysis is limited to a single maneuver in the vertical plane, the effects of fast controls and angular rates on the slow timescale solution will be discussed in Sec. IV in a more general context.

III. Inverse Simulation Algorithm

The procedure adopted for solving the inverse problem on the two timescales is briefly presented inasmuch as only the necessary modifications to the algorithm for its application to dynamic systems such as a rotorcraft are reported in detail. A complete description of the technique may be found in Ref. 11.

Slow Timescale

The governing equations in the slow timescale are Eqs. (1) and (2), and the collective is the primary force generating control. At a given time t_0, the trajectory can be approximated in the Frenet triad by a cubic helix[19] $\boldsymbol{\xi}(s)$, where $s=0$ at $t=t_0$, which is a function of the curvature and torsion evaluated at time t_0. Consequently, the slow timescale state vector can be expressed as

$$\bar{\boldsymbol{x}}_S(t) = \begin{bmatrix} 0 \\ \boldsymbol{R}(t_0) \end{bmatrix} + \begin{bmatrix} \boldsymbol{L}_{IF}(t_0) & 0 \\ 0 & \boldsymbol{L}_{IF}(t_0) \end{bmatrix} \begin{bmatrix} \dot{\boldsymbol{\xi}}(t-t_0) \\ \boldsymbol{\xi}(t-t_0) \end{bmatrix} \tag{18}$$

where the expressions for $\boldsymbol{\xi}$ and the transformation matrix $\boldsymbol{L}_{IF}$ are given in the Appendix. Equation (18) represents an approximation to the solution of Eq. (11) between t_0 and t.

As observed in Ref. 11, the normal unit vector of the Frenet triad is not defined when the flight is rectilinear. Similarly, in the hovering flight of the helicopter, the tangent unit vector is also undefined. Such circumstances, where the Frenet frame is undetermined, are dealt with by expressing the trajectory as

$$\boldsymbol{R}(t) = \boldsymbol{R}(t_0) + (\dot{\boldsymbol{R}}/V)_0 s(t-t_0) \qquad \boldsymbol{R}(t) = \boldsymbol{R}(t_0)$$

for rectilinear and hovering flight, respectively. Because the preceding relations are already written in the inertial frame, the transformation matrix $\boldsymbol{L}_{IF}$ needs not be expressed. Note that the Frenet frame has an instantaneous rotation of 180 deg about the tangent axis when the trajectory presents an inflection point between two arcs that lie on the same plane. The resulting discontinuity on certain elements of $\boldsymbol{L}_{IF}$ has no effect on the accuracy of the inverse solution, as will be shown in the next section where the assigned trajectories for the hurdle-hop and slalom maneuvers have two and three inflection points, respectively.

In the algorithm for the solution of the slow timescale inverse problem that relies on the preceding expansion, the control vector $\tilde{\boldsymbol{u}}_S(t_{i-1/2})$ is determined by a constrained optimization algorithm such that the condition $\boldsymbol{y}_S(t_i) = \boldsymbol{y}_{S_{\text{des}}}(t_i)$ is satisfied,[11] where t_{i-1} and t_i are the bounds of the ith discretization interval, the duration of which is Δt. Note that, because $\boldsymbol{y}_S \in R^3$ and $\tilde{\boldsymbol{u}}_S \in R^4$, that is, the number of controls is larger than the number of constrained outputs, an additional constraint or a penalty index is to be introduced. As a final step, the control $\tilde{\boldsymbol{u}}_S$ is interpolated by a third-order polynomial in the interval $[t_{i-1}, t_i]$ so that the control law for δ_C and the desired outputs for the inner problem are C^1 continuous.

Fast Timescale

In the inner problem [Eq. (13)] the controls are the cyclic stick and the pedals because they generate moments as primary effects. We determine the control $\boldsymbol{u}_F(t)$ that realizes the desired output $\boldsymbol{y}_{F_{\text{des}}} = [\bar{\phi}(t), \bar{\theta}(t), \bar{\psi}(t)]^T$ over the interval Δt. In so doing, as a preliminary step, the commanded attitude is filtered by a second-order dynamics[11] to have a smooth variation of $\dot{\boldsymbol{\omega}}$ (function of $\dot{\boldsymbol{y}}_F$) and, therefore, of $\boldsymbol{u}_F$ at the bounds of the interval $[t_{i-1}, t_i]$. The solution of the inner inverse problem, where the number of controls in $\boldsymbol{u}_F \in R^3$ equals the number of constrained outputs in $\boldsymbol{y}_{F_{\text{COM}}} \in R^3$, is obtained using the integration method of Ref. 18, by assuming that the control vector $\boldsymbol{u}_F$ is piecewise constant in the interval $\delta t = \Delta t/N$.

Note that such aspects as position and rate saturation of the controls can be efficiently dealt with by the optimization algorithm on both the slow and fast timescales.[11]

IV. Results and Discussion

A readily available, six-degrees-of-freedom model of the Bell AH-1G rotorcraft[20] was chosen for this study. The nonlinear model of the vehicle features the quasi-steady, tip-path plane approximation of rotor flapping dynamics, a nonuniform inflow with quasi-steady dynamics, and a detailed description of the aerodynamics of the fuselage and stabilizing surfaces. The total range of control inputs is specified as[21] $|\delta_A| \le 0.152$, $|\delta_B| \le 0.152$, $|\delta_P| \le 0.083$, and $-0.025 \le \delta_C \le 0.127$ m.

For the purposes of the present application, the engine dynamics and the stability augmentation system were not included in the model. The former simplification limits the field of application of the technique to low-to-moderate frequency motions because the engine dynamics, for example, plays a role in aggressive rolling maneuvers. Of course, the solution of the simple inverse problem where a model with first-order engine dynamics is used[16] would be straightforward in the slow timescale discretization interval. Note that a more detailed description of rotorspeed and associated engine and rotor dynamics requires that the slow timescale model is augmented by third-order nonlinear dynamics.[9,20] In that circumstance, we expect a significant increase of computer time to solve the outer problem because the additional states are to be determined by numerical integration, even though the algebraic expression (18) still holds for the trajectory variables.

Next, a linearized form of the aerodynamic forces and moments was used. This approach, which is frequently adopted when low bandwidth control tasks are dealt with (for instance in Ref. 4), allows for an immediate expression of the fast controls in the slow timescale. In this respect, Eq. (8) yields the linear set of equations

$$\begin{bmatrix} L_e/I_x \\ M_e/I_y \\ N_e/I_z \end{bmatrix} + \boldsymbol{D}_S \begin{bmatrix} \bar{u}' \\ \bar{v}' \\ \bar{w}' \\ \bar{\delta}_C' \end{bmatrix} + \boldsymbol{D}_{F_\omega} \bar{\boldsymbol{\omega}}' + \boldsymbol{D}_{F_\delta} \bar{\boldsymbol{u}}_F' = 0 \tag{19}$$

where the trim moments L_e, M_e, and N_e are given by Eqs. (3) written at steady state, the apex indicates variations with respect to the trim values, and

$$\boldsymbol{D}_S = \begin{bmatrix} \mathcal{L}_u & \mathcal{L}_v & \mathcal{L}_w & \mathcal{L}_{\delta_C} \\ \mathcal{M}_u & \mathcal{M}_v & \mathcal{M}_w & \mathcal{M}_{\delta_C} \\ \mathcal{N}_u & \mathcal{N}_v & \mathcal{N}_w & \mathcal{N}_{\delta_C} \end{bmatrix}$$

$$\boldsymbol{D}_{F_\omega} = \begin{bmatrix} \mathcal{L}_p & \mathcal{L}_q & \mathcal{L}_r \\ \mathcal{M}_p & \mathcal{M}_q & \mathcal{M}_r \\ \mathcal{N}_p & \mathcal{N}_q & \mathcal{N}_r \end{bmatrix}, \qquad \boldsymbol{D}_{F_\delta} = \begin{bmatrix} \mathcal{L}_{\delta_A} & \mathcal{L}_{\delta_B} & \mathcal{L}_{\delta_P} \\ \mathcal{M}_{\delta_A} & \mathcal{M}_{\delta_B} & \mathcal{M}_{\delta_P} \\ \mathcal{N}_{\delta_A} & \mathcal{N}_{\delta_B} & \mathcal{N}_{\delta_P} \end{bmatrix}$$

To determine $\bar{\boldsymbol{u}}_F$ we use Eqs. (19) and (9), so that Eq. (10) gives

$$\bar{\boldsymbol{u}}_F' = -\boldsymbol{D}_{F_\delta}^{-1} \left(\begin{bmatrix} L_e/I_x \\ M_e/I_y \\ N_e/I_z \end{bmatrix} + \boldsymbol{D}_S \begin{bmatrix} \bar{u}' \\ \bar{v}' \\ \bar{w}' \\ \bar{\delta}_C' \end{bmatrix} \right) \tag{20}$$

Finally, note that, according to the two-timescale approach discussed in Sec. II, the moments generated by the angular rates are accounted for in the fast timescale.

To demonstrate the capabilities of the two-timescale inverse simulation method, four typical maneuvers are discussed, that is, hurdle-hop, slalom, side-step, and 180-deg level turn.

A discretization interval $\Delta t = \frac{1}{4}$ s is used for the slow timescale inverse problem, whereas $\delta t = \frac{1}{16}$ s is adopted for the fast timescale. The time step of the fourth-order Runge–Kutta method is $\delta\eta = \frac{1}{32}$ s.

In Figs. 3, 5, 7, 9, and 11 the time response computed by the forward integration of the full set of governing equations [Eqs. (1–4)], using the two-timescale solution of the inverse problem as control input, is labeled forward simulation (FS) TSS. When the input to the forward simulation of the vehicle is calculated by the local optimization (LO) method,[18] the results labeled FS LO are also reported for the sake of comparison. In the latter case, where the TSS

approach is not adopted, the discretization interval and the time step for numerical integration are equal to $\frac{1}{16}$ and $\frac{1}{32}$ s, respectively, and a time-delay of 0.5 s in the evaluation of the constrained outputs is necessary to find converged solutions of the optimization problem during the whole maneuver.[18] Finally, the control values are expressed, in Figs. 2, 4, 6, and 8, as fraction of full range displacement ($-1 \le \delta_A, \delta_B, \delta_P \le 1; 0 \le \delta_C \le 1$).

In the hurdle-hop maneuver, the trajectory is assigned as follows:

$$V_{\text{des}}(t) = 30\ \text{ms}^{-1}, \qquad R_{E_{\text{des}}}(t) = 0\ \text{m}$$

$$R_{D_{\text{des}}}(t) = -100 - \frac{40}{16}\left\{8 + \cos\left[\frac{6\pi(t-1)}{20}\right] - 9\cos\left[\frac{2\pi(t-1)}{20}\right]\right\}\text{m}, \qquad \text{for} \qquad 1 < t < 21\ \text{s}$$

$$R_{D_{\text{des}}}(t) = -100\ \text{m}, \qquad \text{for} \qquad t \le 1, \quad t \ge 21\ \text{s}$$

and the further constraint $\beta = 0$ is enforced in the slow timescale. The flight path is realized using the collective as primary control, with negligible variations of roll and yaw angles. The pertinent results are reported in Figs. 2 and 3. In particular, Fig. 2 shows the four control variables as computed by the two-timescale inverse method. Comparison of the δ_B and δ_A plots (Figs. 2b and 2c) with the applied change of δ_C (Fig. 2a) indicates that cyclic controls are almost entirely dedicated to balance the moments generated by the collective input variation. This is also relevant when the variation of longitudinal stick input is interpreted because it appears that, to maintain constant flight speed, a large, forward stick displacement (nose-down) is required.[1,4,9] In fact, in the first phase of the maneuver ($t < 10$ s), it is necessary to manage pitch attitude in the presence of a powerful nose-up pitch moment generated by the collective input. Note that a significantly smaller δ_B variation can be obtained when, in a more likely situation from a real-flight point of view, the forward speed is allowed to decrease.

Figures 2b and 2c also show $\bar{\delta}_B$ and $\bar{\delta}_A$ [slow timescale (TS)] obtained by the solution of the algebraic set of Eq. (20) where $\bar{\delta}_{B,A} = \delta_{B,A_e} + \bar{\delta}'_{B,A}$. The discrepancy between the inner (fast TS) and outer (slow TS) solutions for δ_B and δ_A is due to the effect of both q and $\dot{q}$. For the behavior of δ_P in Fig. 2d, we have that the pedal command has to compensate for yaw moments generated by collective and longitudinal cyclic inputs, where N_{δ_C} and N_{δ_B} are 14.4 and 16.8 $\text{m}^{-1}\text{s}^{-2}$, respectively. The poor match between δ_P computed in the two timescales is mainly caused by the differences of the longitudinal cyclic command in the fast and slow TS.

Next, Figs. 3a, 3c, and 3d, where the constrained outputs V, R_D and R_E, respectively, are reported, show that the error with respect to the desired values (des) of the states is practically negligible. The differences between the solutions obtained by the actual technique (FS TSS) and the method of Ref. 18 (FS LO) are also very small, and we note in Fig. 3c the effect of the aforementioned time delay.[11,18] The pseudocontrols $\bar{\phi}$, $\bar{\theta}$, and $\bar{\psi}$ (slow TS) in Fig. 3b are accurately achieved when the computed controls are the input for the forward simulation of the maneuver (FS TSS). In Fig. 3b we also observe that a nose-up pitch angle variation is initially realized to control speed as the helicopter pushes over.

A two-sided slalom maneuver consists of a rapid sequence of turns in the horizontal plane. The trajectory is assigned as follows:

$$V_{\text{des}}(t) = 30\,\text{ms}^{-1}$$

$$R_{E_{\text{des}}}(t) = \frac{50}{27\sqrt{3}}\left\{32\sin\left[\frac{2\pi(t-5)}{30}\right] - 20\sin\left[\frac{4\pi(t-5)}{30}\right] + 2\sin\left[\frac{8\pi(t-5)}{30}\right]\right\}\text{m}, \qquad \text{for} \qquad 5 < t < 35\ \text{s}$$

$$R_{E_{\text{des}}}(t) = 0\,\text{m}, \qquad \text{for} \qquad t \le 5, \quad t \ge 35\ \text{s}$$

$$R_{D_{\text{des}}}(t) = -100\,\text{m}$$

and we have $\beta = 0$ in the outer problem. The aspect ratio of the slalom, that is, the overall width over length ratio, is equal to 0.118. The control variables and some of the states are shown in Figs. 4 and 5. We observe in Figs. 4b–4d that the fast controls computed in the slow TS are slightly changed with respect to the trim value at $t = 0$ because the collective input variation is more limited than in the hurdle-hop maneuver. On the other hand, unlike the preceding maneuver where the required acceleration is mainly obtained by rotor disk tilting, the variation of $\boldsymbol{u}_F$ in the inner problem (fast TS) is more relevant to generate large values of roll and pitch rates as required for a significant tilting of the rotor force, whereas the large variation of the yaw angle (Fig. 5b) is caused by the constraint $\beta = 0$. For the angular velocity components, we have $|p| \le 18$, $|q| \le 6$, and $|r| \le 10$ deg s^{-1}. Figure 5d shows that the assigned ground track is achieved with good accuracy, although a small error of 4 m is visible at the exit of the maneuver,

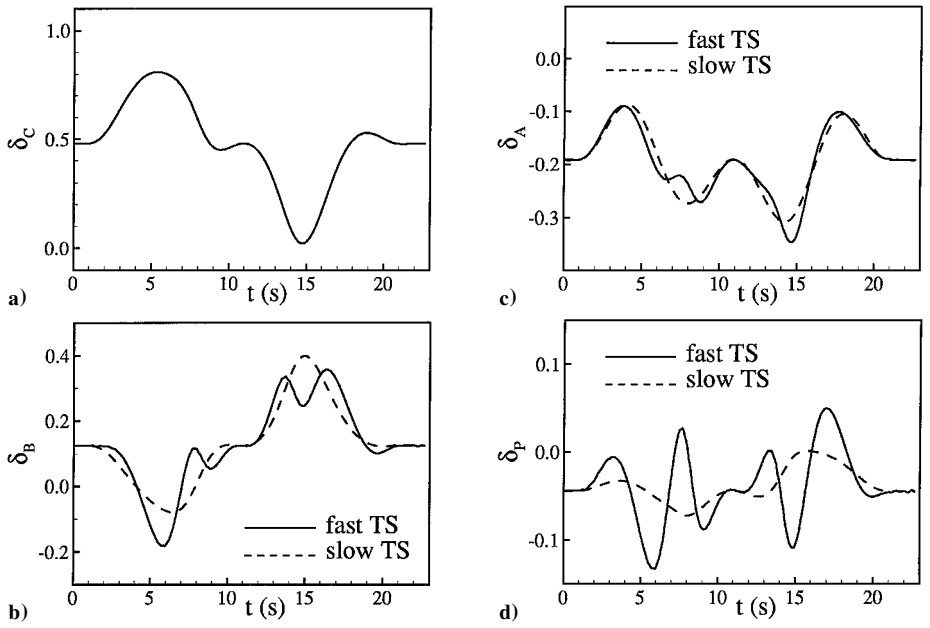

Fig. 2 Hurdle-hop maneuver: control variables.

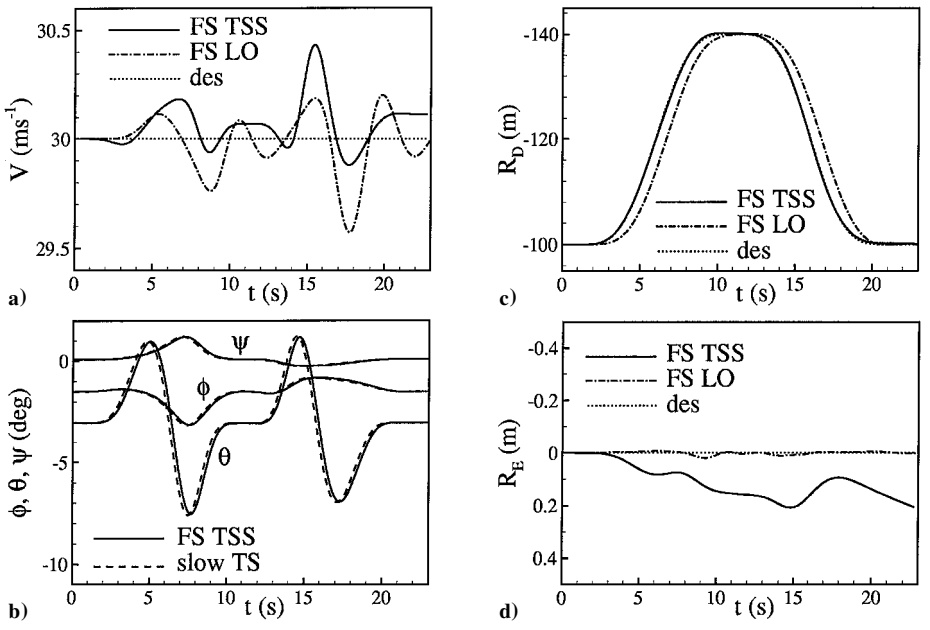

Fig. 3 Hurdle-hop maneuver: state variables and specified outputs.

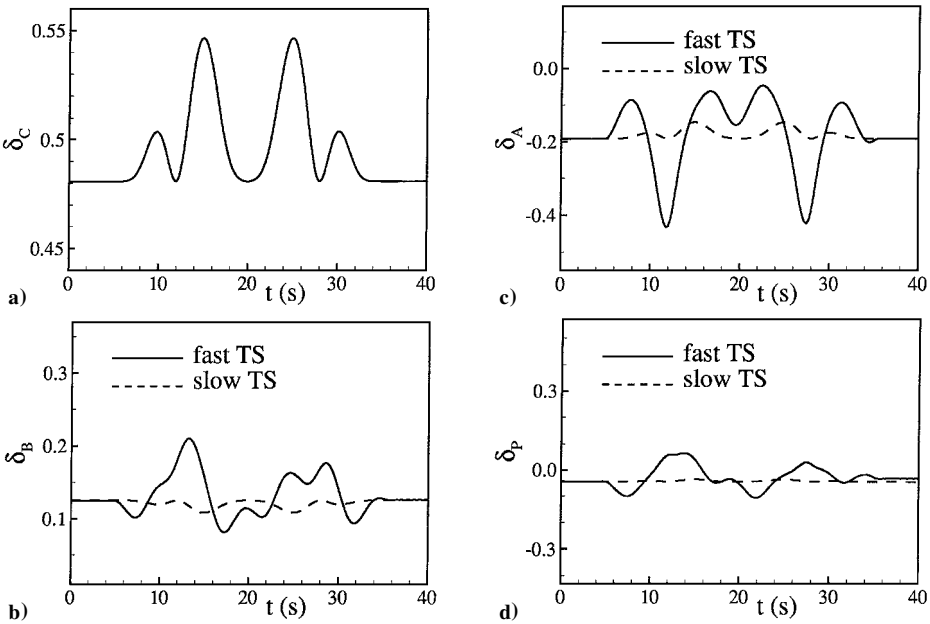

Fig. 4 Slalom maneuver (β = 0): control variables.

the duration of which is 30 s. Finally, Figs. 5a and 5c confirm that the constrained values of V and R_D are also realized with negligible errors.

The same slalom maneuver is solved by constraining the yaw angle, that is, $\psi = \psi_e$, where $\psi_e = 0.1$ deg. The control displacements over full range are shown in Fig. 6, and the sideslip angle and aircraft attitude are reported in Fig. 7. Not shown, the assigned trajectory is precisely tracked, with the final error on both R_E and R_D of the order of a few meters. In Fig. 7a, we see that large values of β are necessary to maintain the nose pointed in a constant direction. In comparison with the preceding situation, where a sequence of banked turns was executed, the roll angle is slightly modified from the trim value while pitch angle variations in the range $-10.1 \leq \theta \leq 4.5$ deg are required. It is interesting to observe in Figs. 6b–6d that the fast control displacements in the outer problem (slow TS) are used to balance the moments generated by the sideslip angle. This effect is particularly noticeable for δ_P because the yaw moment due to the lateral velocity v is much higher than the moment determined by the longitudinal cyclic variation in the fast TS. As a result, with the yaw rate nearly equal to zero during the maneuver, we have rather small difference between the slow and fast TS solutions in Fig. 6d.

The next maneuver is a side-step starting in hovering. The pertinent constraints are

$$R_{N_{\text{des}}}(t) = 0 \text{ m}$$

$$R_{E_{\text{des}}}(t) = 0 \text{ m}, \qquad \text{for} \qquad t \leq 1 \text{ s}$$

$$R_{E_{\text{des}}}(t) = \frac{15}{16}\left\{8 + \cos\left[\frac{3\pi(t-1)}{10}\right] - 9\cos\left[\frac{\pi(t-1)}{10}\right]\right\} \text{m} \qquad \text{for} \qquad 1 < t < 11 \text{ s}$$

$$R_{E_{\text{des}}}(t) = 15 \text{ m}, \qquad \text{for} \qquad t \geq 11 \text{ s}$$

$$R_{D_{\text{des}}}(t) = -100 \text{ m}$$

with the additional condition $\psi(t) = \psi_e = -2.6$ deg for the slow TS inverse problem. Figure 8 shows the control variables (over full range displacement) and the slow TS value of $\boldsymbol{u}_F$. Note in Fig. 8c the sizeable difference between $\bar{\delta}_A$ (slow TS) and its inner value

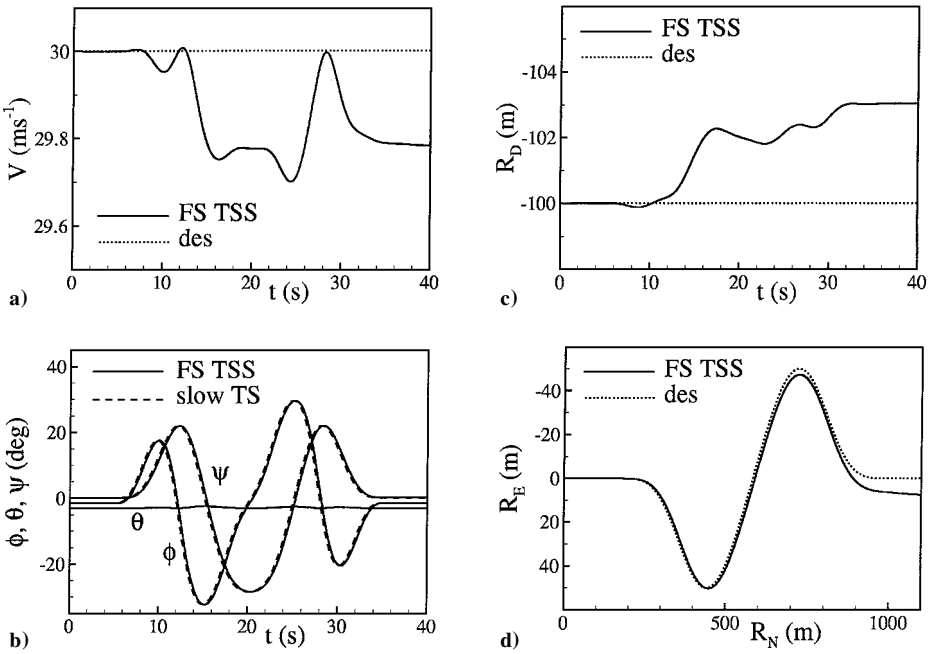

Fig. 5 Slalom maneuver ($\beta = 0$): state variables and specified outputs.

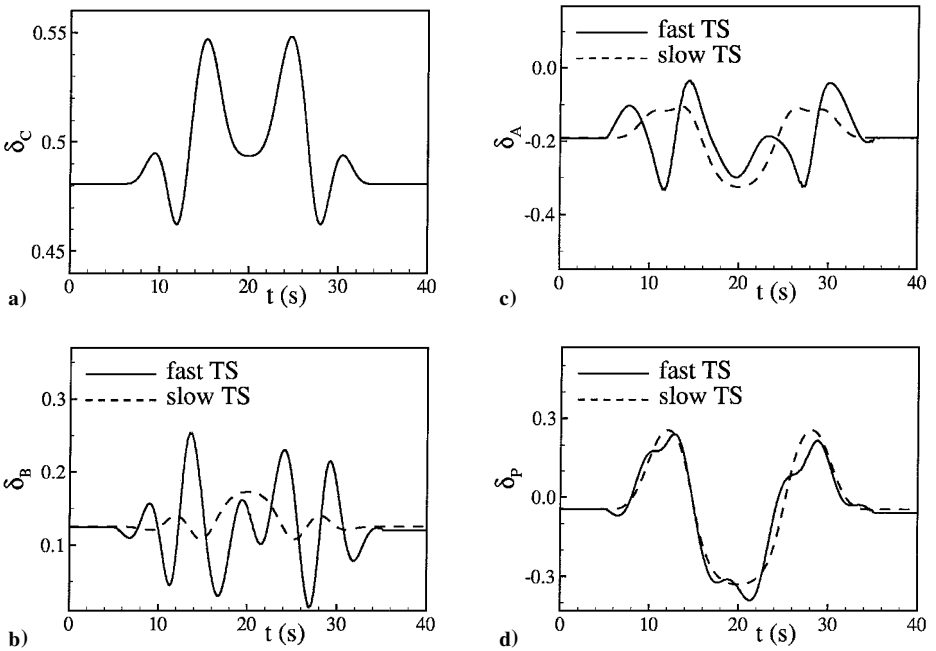

Fig. 6 Slalom maneuver ($\psi = \psi_e$): control variables.

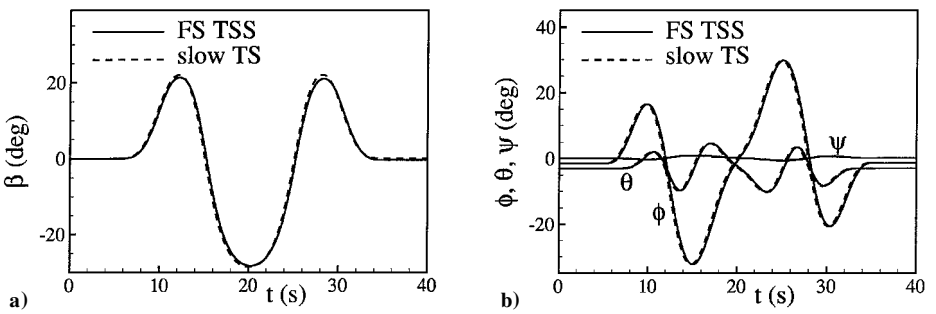

Fig. 7 Slalom maneuver ($\psi = \psi_e$): state variables.

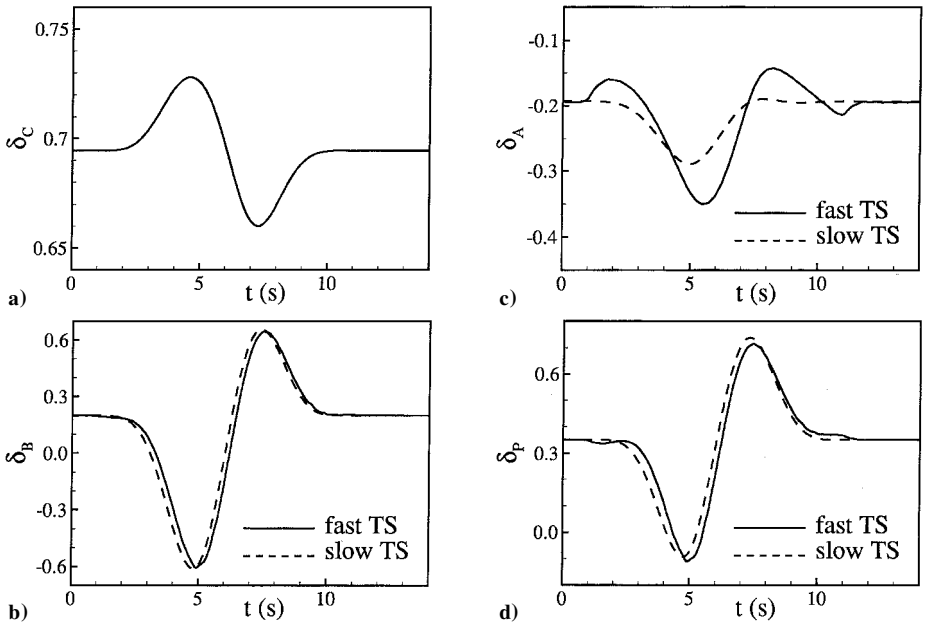

Fig. 8 Side-step maneuver: control variables.

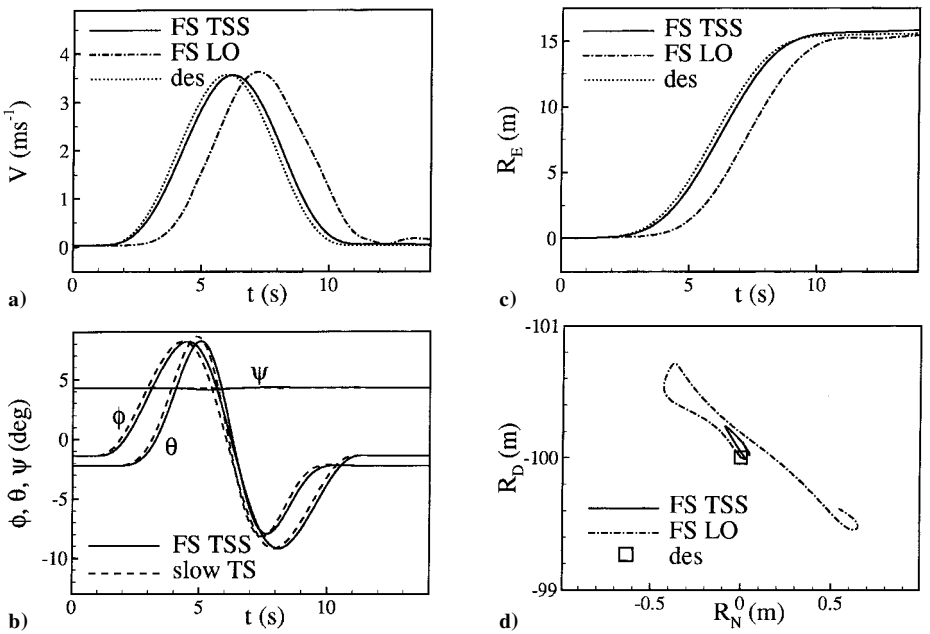

Fig. 9 Side-step maneuver: state variables and specified outputs.

(fast TS). This situation, already observed in the slalom maneuver at $\beta = 0$ for all of the fast controls, is due to the assumption $\bar{p} = 0$ in the outer problem when the maneuver is characterized by a prompt generation of roll rate through lateral cyclic input. The longitudinal cyclic and pedal displacement in the two TS are nearly indistinguishable because the principal effect of these control inputs is to balance pitch and yaw moments due to sideslip.

The discrepancies between the achieved values of the constrained variables (FS TSS), the assigned values (des) and the results of the method in Ref. 18 (FS LO) appear negligible in Figs. 9a, 9c, and 9d. In Fig. 9a we observe, again, the effect of the time delay required for the application of the local optimization technique[18] (FS LO). Finally, Fig. 9b shows that the control generated Euler angles (FS TSS) are in good agreement with the pseudocontrols $\bar{\phi}$, $\bar{\theta}$, and $\bar{\psi}$ resulting from the outer problem solution (slow TS).

The issue of the relative importance of control vs angular rate terms in the outer solution, already analyzed at the end of Sec. II, is worth some additional comments. In most of the reported results it appears that the fast control displacements computed in the slow TS ($\bar{\boldsymbol{u}}_F$) are rather different from their value obtained from the solution of the fast TS inverse problem ($\boldsymbol{u}_F$). Such a poor agreement could raise the question whether it is meaningful to determine $\bar{\boldsymbol{u}}_F$ in the inverse solution of the outer problem. To address this point, we consider a fourth maneuver, that is, a level turn at increasing speed.

Starting from a rectilinear flight at $R_D = -100$ m and $V = 30$ m s^{-1}, either a 180-deg left-hand or right-hand turn is executed, to account for the asymmetry of the vehicle, while the velocity is increased to 40 m s^{-1}. Figure 10 reports $\Delta R/\Delta s$, where $\Delta R = \|\boldsymbol{R}(t) - \boldsymbol{R}_{\text{des}}(t)\|$ is a measure of the position error, $\boldsymbol{R}(t)$ is the control generated flight path, obtained by forward simulation, and Δs is the distance covered along the trajectory. The maneuver time is $T = 40$ s in Fig. 10a and $T = 20$ s in Fig. 10b, and the maximum values of the angular velocity components are 8 deg s^{-1} for p and 14 deg s^{-1} for q, respectively. The label $\bar{\boldsymbol{u}}_F = 0$ (dotted lines) indicates that the control displacements required to fly the assigned flight path are determined neglecting the force generated by the fast

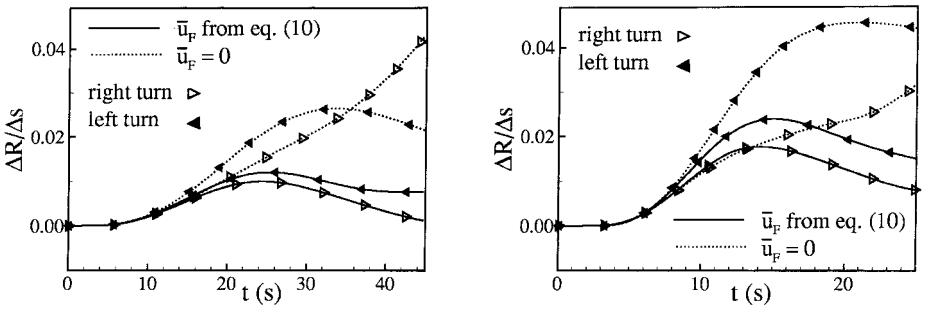

a) $T = 40$ s b) $T = 20$ s

Fig. 10 Effect of $\bar{u}_F$ in 180-deg turns with acceleration.

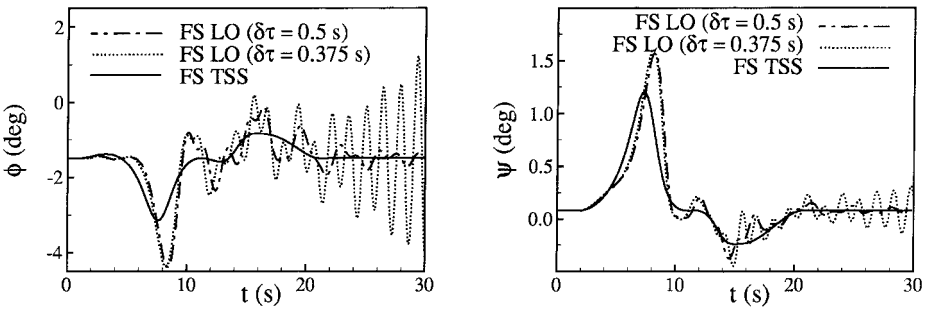

Fig. 11 Hurdle-hop maneuver: roll and yaw angles computed by the two-TS method (FS TSS) and the technique of Ref. 18 (FS LO).

controls in the outer problem, whereas the continuous lines show the position error when the contribution to the total force of the terms depending on $\bar{\boldsymbol{u}}_F$ is accounted for.

First, it was already demonstrated in Sec. II for the hurdle-hop maneuver that the inverse solution of the outer problem is slightly influenced by the body force due to angular rate and acceleration. The small effect of $\boldsymbol{u}_F - \bar{\boldsymbol{u}}_F$ on the trajectory variables is confirmed when a more complex, three-dimensional flight path is flown because Fig. 10 (continuous lines) shows that, in all of the circumstances, the position error is small at the exit from the maneuver although, as expected, the maximum value of ΔR is higher for the turn of shorter duration, where the angular rates are larger.

Next, it is apparent that the control inputs obtained by the TSS method when $\bar{\boldsymbol{u}}_F$ is set to zero in the slow TS cause large position errors with respect to the desired trajectory, such that the specified trim conditions are not recovered at the exit from right turns. In particular, in situations where the final trim condition is different from the steady state at the beginning of the maneuver ($0 \le t \le 2.5$ s), so that a nonzero $\bar{\boldsymbol{u}}'_F$ results at $t = T$, neglecting of the force terms due to the fast controls yields a noticeable error on the pseudocontrols $\bar{\phi}$, $\bar{\theta}$, and $\bar{\psi}$. As a consequence, when forward simulation is carried out using the controls computed by the TSS inverse method, the rotor thrust vector is incorrectly pointed and, in most cases, no steady state is achieved at the end of the maneuver.

As already mentioned, conjugate transmission zeros produce nonobservable oscillatory motions that, among other effects, prevent the recovery of a steady-state flight condition after the maneuver is completed. To clarify this, we note that the AH-1G helicopter model, in the reference condition of rectilinear flight at $V = 30$ m s^{-1}, has two pairs of transmission zeros when the output vector is $\boldsymbol{y} = (R_N, R_E, R_D, \beta)^T$, that is, $z_{T_{1,2}} = 0.10 \pm 5.32j$ s^{-1} and $z_{T_{3,4}} = -0.078 \pm 2.06j$ s^{-1}. Figure 11 reports the roll and yaw angles achieved using the inverse solution of the hurdle-hop maneuver provided by the method of Ref. 18 (FS LO) as control input, where the full dynamics of the system are taken into consideration. The maneuver is completed at $t = 21$ s, and the input law is determined until $t = 30$ s because the specified outputs are at the reference value for $t \ge 21$. Although the desired values of the assigned outputs are obtained, we see amplitude oscillations in the considered states ($\delta\tau = 0.5$ s) the period of which is equal to 1.4 s, related to $z_{T_{1,2}}$, and the response is diverging as the time delay $\delta\tau$ is decreased. On the other hand, when the inverse simulation is carried out by the present method on the two subsystems of the slow and fast dynamics (FS TSS), none of which has transmission zeros, it is apparent that the steady-state values of ϕ and ψ are accurately obtained.

Therefore, the effects of nonobservable motions should be carefully considered when the output variables are to be specified in inverse simulation algorithms based on the integration method, whereas the TSS approach rules out this problem. In this respect and in a more general context, whenever reference is made to problems associated with uncontrollable states as, for instance, in Refs. 9 and 12, the transmission zeros of the system should be analyzed.

Finally, the CPU time on a Pentium II, 350-MHz personal computer was evaluated for the present algorithm and the local optimization method.[18] The time required by the integration method of Ref. 18 was 38.1 s for the hurdle-hop maneuver and 23.6 s for the side-step maneuver. On the other hand, the two-TS algorithm uses 3.0 and 1.7 s of CPU time, respectively, for the same maneuvers, thus allowing for an order of magnitude reduction of the computational time. Note that the CPU time is rather insensitive to the time interval of the slow dynamics. For instance, using Δt as short as 0.12 s gives 3.3 and 2.0 s for the inverse solution of the hurdle-hop and side-step maneuvers, respectively.

V. Conclusions

An inverse simulation technique, based on the concept of TS separation, has been adapted and evaluated for the study of helicopter maneuvers.

The two-time-scale method accounts for the relevant effect of the force generated by cyclic stick and pedals and appears suitable and very effective as far as the accuracy and numerical stability of the method and the time taken to produce a solution at convergence are concerned. In particular, the algorithm is about an order of magnitude faster than the numerical integration methods and should provide equivalent performances in comparison to differentiation algorithms that reportedly can be run in real time.

The calculation scheme is rather flexible because the vehicle performance can be determined in different situations, where, for instance, zero sideslip angle as well as zero heading change are specified in slalom maneuvers, according to pilot perspective.

Finally, the proposed technique prevents the relevant issue of nonobservable motions that exist as the helicopter trajectory is specified in terms of c.g. coordinates and in so doing allows the full recovery of a steady-state flight condition at the exit of the maneuver.

Appendix: Trajectory Expansion

The expression of $\boldsymbol{\xi}$ is[17]

$$\boldsymbol{\xi}(s) = \begin{bmatrix} s - s^3\left(k_1^2\right)_0/3! \\ s^2(k_1)_0/2! + s^3(\mathrm{d}k_1/\mathrm{d}s)_0/3! \\ s^3(k_1k_2)_0/3! \end{bmatrix}$$

The curvilinear abscissa s is written as

$$s(t-t_0) = V_0(t-t_0) + \dot{V}_0(t-t_0)^2/2! + \ddot{V}_0(t-t_0)^3/3!$$

whereas the expressions of the curvature and torsion, k_1 and k_2, are[19]

$$k_1 = \frac{1}{V^2}(|\ddot{\boldsymbol{R}}|^2 - \dot{V}^2)^{\frac{1}{2}}, \qquad k_2 = \frac{\det\{\dot{\boldsymbol{R}}, \ddot{\boldsymbol{R}}, \dddot{\boldsymbol{R}}\}}{V^2(|\ddot{\boldsymbol{R}}|^2 - \dot{V}^2)}$$

and $\mathrm{d}k_1/\mathrm{d}s = \dot{k}_1/V$. The transformation matrix $\boldsymbol{L}_{IF}$ from the Frenet frame to the inertial frame is given by

$$\boldsymbol{L}_{IF}(t_0) = (\dot{\boldsymbol{R}}/V, \boldsymbol{n}/|\boldsymbol{n}|, \tilde{\boldsymbol{R}}\boldsymbol{n}/V|\boldsymbol{n}|)_0$$

where the first, second, and third derivatives of $\boldsymbol{R}$ are to be computed at t_0 to evaluate $\boldsymbol{\xi}$. In this respect, $\dot{\boldsymbol{R}}_0$ and $\ddot{\boldsymbol{R}}_0$ are given by Eqs. (2) and (1), respectively. The third derivative of $\boldsymbol{R}_0$ is computed by numerical differentiation. In the preceding equation, $\boldsymbol{n} = \ddot{\boldsymbol{R}} - \dot{\boldsymbol{R}}\dot{V}/V$, and $\tilde{\boldsymbol{R}}\boldsymbol{n}$ is the matrix equivalent of vector product.

Acknowledgment

This work was partially supported by the Italian National Program of Researches in Antarctica.

References

[1]Thomson, G. D., "Evaluation of Helicopter Agility Through Inverse Solution of the Equations of Motion," Ph.D. Dissertation, Dept. of Aerospace Engineering, Univ. of Glasgow, Glasgow, Scotland, U.K., May 1987.

[2]Bradley, R., Padfield, G. D., Murray-Smith, D. J., and Thomson, D. G., "Validation of Helicopter Mathematical Models," *Transactions of the Institute of Measurements and Control*, Vol. 12, No. 4, 1990, pp. 186–196.

[3]Whalley, M. S., "Development and Evaluation of an Inverse Solution Technique for Studying Helicopter Maneuverability and Agility," NASA TM 102889, July 1991.

[4]Hess, R. A., and Gao, C., "A Generalized Algorithm for Inverse Simulation Applied to Helicopter Maneuvering Flight," *Journal of the American Helicopter Society*, Vol. 38, No. 4, 1993, pp. 3–15.

[5]Thomson, D. G., Taylor, C. D., Talbot, N., Ablett, R., and Bradley, R., "An Investigation of Piloting Strategies for Engine Failures During Takeoff from Offshore Platforms," *Aeronautical Journal*, Vol. 99, No. 981, 1995, pp. 15–25.

[6]Thomson, D. G., and Bradley, R., "The Use of Inverse Simulation for Preliminary Assessment of Helicopter Handling Qualities," *Aeronautical Journal*, Vol. 101, No. 1007, 1997, pp. 287–294.

[7]Boyle, D., and Chamitoff, G., "Autonomous Maneuver Tracking for Self-Piloted Vehicles," *Journal of Guidance, Control, and Dynamics*, Vol. 22, No. 1, 1999, pp. 58–67.

[8]Lee, S., and Kim, Y., "Time-Domain Finite Element Method for Inverse Problem of Aircraft Maneuvers," *Journal of Guidance, Control, and Dynamics*, Vol. 20, No. 1, 1997, pp. 97–103.

[9]Rutheford, S., and Thomson, D. G., "Improved Methodology for Inverse Simulation," *Aeronautical Journal*, Vol. 100, No. 993, 1996, pp. 79–86.

[10]Yip, K. M., and Leng, G., "Stability Analysis for Inverse Simulation of Aircraft," *Aeronautical Journal*, Vol. 102, No. 1016, 1998, pp. 345–351.

[11]Avanzini, G., de Matteis, G., and de Socio, L. M., "Two Timescale Integration Method for Inverse Simulation," *Journal of Guidance, Control, and Dynamics*, Vol. 22, No. 3, 1999, pp. 395–401.

[12]Lin, K. C., Lu, P., and Smith, M., "The Numerical Errors in Inverse Simulation," AIAA Paper 93-3588, Aug. 1993.

[13]Rutheford, S., and Thomson, D. G., "Helicopter Inverse Simulation Incorporating an Individual Blade Rotor Model," *Journal of Aircraft*, Vol. 36, No. 5, 1997, pp. 627–634.

[14]Chen, F. C., and Khalil, H. K., "Two-Timescale Longitudinal Control of Airplanes Using Singular Perturbation," *Journal of Guidance, Control, and Dynamics*, Vol. 13, No. 6, 1990, pp. 952–960.

[15]Snell, S. A., Enns, D. F., and Garrard W. L., "Nonlinear Inversion Control for a Supermaneuverable Aircraft," *Journal of Guidance, Control, and Dynamics*, Vol. 15, No. 4, 1992, pp. 976–984.

[16]Heiges, M. W., Menon, P. K. A., and Schrage, D. P., "Synthesis of a Helicopter Full-Authority Controller," *Journal of Guidance, Control, and Dynamics*, Vol. 15, No. 1, 1992, pp. 222–227.

[17]Avanzini, G., de Matteis, G., and de Socio, L. M., "Natural Description of Aircraft Motion," *Journal of Guidance, Control, and Dynamics*, Vol. 21, No. 2, 1998, pp. 229–233.

[18]de Matteis, G., de Socio, L. M., and Leonessa, A., "Solution of Aircraft Inverse Problems by Local Optimization," *Journal of Guidance, Control, and Dynamics*, Vol. 18, No. 3, 1995, pp. 567–571.

[19]Kepr, B., "Differential Geometry," *Survey of Applicable Mathematics*, edited by K. Rektorys, MIT Press, Cambridge, MA, 1969, pp. 306–317.

[20]Talbot, P. D., Tinling, B. E., Decker, W. A., and Chen, R. T., "A Mathematical Model of a Single Main Rotor Helicopter for Piloted Simulation," NASA TM-84281, Sept. 1982.

[21]Lewis, M. S., "Piloted Simulation of One-on-One Helicopter Air Combat at NOE Flight Levels," NASA TM86686, April 1985.